

Article

# Enthalpies of Hydrate Formation from Hydrate Formers Dissolved in Water

Bjørn Kvamme

Strategic Carbon, Vestre Holbergsallmenningen 17, 5011 Bergen, Norway; bjkvamme@gmail.com;  
Tel.: +47-9345-1956

Received: 21 February 2019; Accepted: 15 March 2019; Published: 18 March 2019



**Abstract:** The international interest in the energy potential related to the huge amounts of methane trapped in the form of hydrates is rapidly increasing. Unlike conventional hydrocarbon sources these natural gas hydrate deposits are widely spread around the world. This includes countries which have limited or no conventional hydrocarbon sources, like for instance Japan. A variety of possible production methods have been proposed during the latest four decades. The pressure reduction method has been dominant in terms of research efforts and associated investments in large scale pilot test studies. Common to any feasible method for producing methane from hydrates is the need for transfer of heat. In the pressure reduction method necessary heat is normally expected to be supplied from the surrounding formation. It still remain, however, unverified whether the capacity, and heat transport capabilities of surrounding formation, will be sufficient to supply enough heat for a commercial production based on reduction in pressure. Adding heat is very costly. Addition of limited heat in critical areas (regions of potential freezing down) might be economically feasible. This requires knowledge about enthalpies of hydrate dissociation under various conditions of temperature and pressure. When hydrate is present in the pores then it is the most stable phase for water. Hydrate can then grow in the concentration range in between liquid controlled solubility concentrations, and the minimum concentration of hydrate in water needed to keep the hydrate stable. Every concentration in that range off concentrations results unique free energy and enthalpy of the formed hydrate. Similarly for hydrate dissociation towards water containing less hydrate former than the stability limit. Every outside liquid water concentration results in unique enthalpy changes for hydrate dissociation. There are presently no other available calculation approaches for enthalpy changes related to these hydrate phase transitions. The interest of using CO<sub>2</sub> for safe storage in the form of hydrate, and associated CH<sub>4</sub> release, is also increasing. The only feasible mechanism in this method involves the formation of new CO<sub>2</sub> hydrate, and associated release of heat which assist in dissociating the *in situ* CH<sub>4</sub> hydrate. Very limited experimental data is available for heats of formation (and dissociation), even for CH<sub>4</sub>. And most experimental data are incomplete in the sense that associated water/hydrate former rate are often missing or guessed. Thermodynamic conditions are frequently not precisely defined. Although measured hydrate equilibrium pressure versus temperature curves can be used there is still a need for additional models for volume changes, and ways to find other information needed. In this work we propose a simple and fairly direct scheme of calculating enthalpies of formation and dissociation using residual thermodynamics. This is feasible since also hydrate can be described by residual thermodynamics though molecular dynamics simulations. The concept is derived and explained in detail and also compared to experimental data. For enthalpy changes related to hydrate formation from water and dissolved hydrate formers we have not found experimental data to compare with. To our knowledge there are no other alternative methods available for calculating enthalpy changes for these types of hydrate phase transitions. And there are no limits in the theory for which hydrate phase transitions that can be described as long as chemical potentials for water and hydrate formers in the relevant phases are available from theoretical modeling and/or experimental information.

**Keywords:** hydrate; phase transitions; enthalpy changes

---

## 1. Introduction

Industrial problems related to hydrate formation in pipelines and process equipment has historically motivated much of the hydrate research. In many of these systems the heat released during hydrate formation is rapidly distributed through liquid water and solid metal. Related kinetic models have therefore typically focused on the thermodynamic driving force and related mass transport. During the few latest decades the interest in natural gas hydrates as an energy source has increased substantially. Any method utilized for production of methane gas from methane gas hydrates will involve transfer of heat. Most efforts has been on reducing the pressure to outside hydrate stability, which addresses the thermodynamic driving force but the heat still needs to be supplied from the surroundings, or added in some other way. Some very short pilot tests have been conducted in Alaska [1,2]. In more recent years two tests were conducted off the shore of Japan. The first one lasted for six days and was stopped due to problems with production of sand and water, as well as a freezing down due to limited heat supply capacity from the surroundings [3]. The second test was designed and planned for six months of continuous production but closed down after 24 days due to freezing down problems [4]. Thermal stimulation, through for instance steam or hot water, is also possible but considered far too expensive as the primary method. A more novel technology is to inject carbon dioxide. A solid state conversion mechanism has been proven by Ripmeester et al. [5] and Kuhs et al. [6] for temperatures far below zero Celsius. For temperatures above zero Celsius a substantially faster mechanism [7,8] involves the formation of a new CO<sub>2</sub> dominated hydrate inside the pores using free pore water. Even in permafrost areas it is hard to find any natural gas hydrate deposits with higher hydrate saturations than 85% of the available pore volume. The more typical is 75% or lower like also in the Ignik Sikimu pilot test [9,10]. Injection of CO<sub>2</sub> will lead to the formation of a new CO<sub>2</sub> hydrate from the free water in the pores and the injected CO<sub>2</sub>. Addition of small amounts of surfactant will keep the interface free of hydrate [11] and stimulate to hydrate nucleation and growth below the CO<sub>2</sub>/water interface region. The effects of surfactant on interface free energy and increased solubility of CO<sub>2</sub> below the surfactant stimulated interface are additional effects that will stimulate hydrate growth from solution. Practically it has been observed that small amounts of methanol will act as promotor for hydrate formation in a pipeline [12].

In view of the above there is a need for consistent and reliable data for enthalpies of hydrate formation or dissociation. As will be discussed in Section 2 available experimental data are very limited and normally incomplete in various ways like for instance missing hydrations number, and unprecise information on thermodynamic conditions. Pressure temperature hydrate equilibrium curves can be measured, or calculated using one of the many codes around the world. With additional data on volumetric changes it is possible to calculate enthalpies of phase transitions. This approach, the so-called Clapeyron method, becomes more complex for mixtures. And the method is not directly usable for hydrate formation from solution of hydrate formers in water. The use of residual thermodynamics, as proposed here, is simple and has no limitations as to which phases water and hydrate formers come from.

A brief review of available experimental data for methane hydrate and carbon dioxide hydrate is given in Section 2. The Clapeyron of using the pressure/temperature gradient, and the simplified Clausius-Clapeyron, have been typical methods for estimating enthalpies of hydrate formation. These methods are briefly discussed in Section 2. The main focus of Section 2, however, is the description of the proposed method for calculating enthalpies of hydrate phase transitions. The method is illustrated and compared to available experimental data. Additional results are presented and discussed in Section 3, followed by discussions in Section 4 and our conclusions in Section 5.

## 2. Methodologies

The use of residual thermodynamics also for water as liquid, ice or in empty clathrates of structures I and II makes it feasible to calculate thermodynamic properties related to hydrate phase transitions in a consistent way since the reference state for all components, in all phases is the same. The use of model molecules and Molecular Dynamics (MD) simulations will directly provide residual properties through samplings in configurational space. Average ideal gas properties are also available through samplings in momentum space. For rigid molecules like those utilized in our work ideal gas properties are trivially available from atomic masses and moments of inertia. In this work we utilize this approach and evaluate calculated results for various properties towards experimental data from open literature. Enthalpies of hydrate formation along pressure temperature equilibrium curves will of course have same values as dissociation enthalpies for the same conditions, but with opposite sign. Extensions to conditions outside equilibrium follow standard thermodynamic relationships and are the subjects of follow-up papers. The first section of methodologies describes the theory for situations in which temperature and pressure are the independent thermodynamic variables. This is the most commonly studied route to hydrate formation from water and a separate hydrate former phase.

For hydrate formation from dissolved hydrate formers the main modifications of the calculation scheme are for the change in hydrate former enthalpy, from a rather dilute solution in water to being captured inside a hydrate cavity. Unlike hydrate formers from a gas (or liquid) the enthalpy changes for hydrate formers in this case is smaller. This is expected since water have to optimize entropy in hydrate bonding structures around these solutes. This results in very cavity like water structures that we, and many other research groups, have reported during the latest three decades. In terms of enthalpies of hydrate formation for homogeneous hydrate formation from water solution we accordingly expect smaller absolute values than for the heterogeneous case.

### 2.1. Residual Thermodynamic Modeling of Hydrate Formation from Water and Separate Hydrate Former Phase

By definition a hydrate phase transition is reversible along the equilibrium curve. This is also utilized for the Clapeyron based methods for the formation of hydrate from a separate gas (or liquid) hydrate former phase and a free water phase. The free energy change for this phase transition can be written as:

$$\Delta G^{(H_1)} = \left[ \begin{array}{l} x_{H_2O}^H \left( \mu_{H_2O}^H(T, P, \vec{x}^H) - \mu_{H_2O}^{water}(T, P, \vec{x}) \right) \\ + \sum_i x_i^H \left( \mu_i^H(T, P, \vec{x}^H) - \mu_i^{gas}(T, P, \vec{y}^{gas}) \right) \end{array} \right] \quad (1)$$

The superscript  $H_1$  is used to distinguish the specific heterogeneous phase transition from other hydrate formation phase transitions.  $T$  is temperature,  $P$  is pressure.  $x$  is the mole-fraction in either liquid or hydrate (denoted with a superscript  $H$ ) while  $y$  is the mole-fraction in gas (or liquid) hydrate former phase.  $i$  is an index for hydrate formers. The superscript *water* denotes a water phase that is converted into hydrate. Generally this is ice or liquid but in this work we only consider liquid water.  $\mu$  is the chemical potential. In subsequent papers this can also be chemical potential for water adsorbed in various distances from a solid mineral surface.

Liquid water chemical potential is calculated from the symmetric excess conventions as:

$$\mu_{H_2O}^{water}(T, P, \vec{x}) = \mu_{H_2O}^{pure, H_2O}(T, P) + RT \ln [x_{H_2O} \gamma_{H_2O}(T, P, \vec{x})] \approx \mu_{H_2O}^{pure, H_2O}(T, P) + RT \ln [x_{H_2O}] \quad (2)$$

$\lim(\gamma_{H_2O}) = 1.0$  when  $x_{H_2O}$  approaches unity

The approximation on the right-hand side is strictly not necessary. We could utilize a theoretical model for the activity coefficient or we could also use Gibbs-Duhem [13] to relate this to the activity of  $CO_2$  in water as we have done in our Phase Field Theory modelling of  $CO_2$  hydrate phase transition dynamics studies [14,15]. Since the focus here is to illustrate the complexity of multiple hydrate formation in systems of water and  $CO_2$  we use a simpler kinetic model which is more visible in terms

of the various contributions to the hydrate phase transition dynamics. As such the approximation on the right-hand side of (2) is accurate enough for the purpose. The solubility of CH<sub>4</sub> in water is small and right hand side will be close to pure water chemical potential.

Chemical potential for water in the hydrate structure is given by [16]:

$$\mu_{H_2O}^H = \mu_{H_2O}^{O,H} - \sum_{k=1,2} RTv_k \ln \left( 1 + \sum_i h_{ij} \right) \quad (3)$$

in which  $H$  denotes hydrate and  $O$  in the superscript on first term on right hand side means empty clathrate. These chemical potentials are readily available from model water (TIP4P) simulations [17]. The number of cavities per water  $v_k$  is 1/23 for small cavities of structure I and 3/23 for large cavities. With CO<sub>2</sub> as only guest  $i$  is 1 in the sum over canonical partition functions for small and large cavities.

$$h_{ki} = e^{\beta[\mu_{ki} - \Delta g_{ki}]} \quad (4)$$

where  $\beta$  is the inverse of the universal gas constant times temperature. At equilibrium chemical potential of guest molecules  $i$  in hydrate cavity  $k$  is equal to the chemical potential of molecules  $i$  in the co-existing phase it comes from. For non-equilibrium the chemical potential is adjusted for distance from equilibrium through a Taylor expansion as discussed later. The free energies of inclusion (latter term in the exponent) are reported elsewhere [11,18–21]. At thermodynamic equilibrium between a free hydrate former phase and the hydrate, then  $\mu_{ki}$  is the chemical potential of the guest molecule in the hydrate former phase (gas, liquid or fluid) at hydrate equilibrium temperature and pressure.

The corresponding filling fractions and mole-fractions of methane in the hydrate is given by:

$$\theta_{ki} = \frac{h_{ki}}{1 + \sum_j h_{kj}} \quad (5)$$

$\theta_{ki}$  is the filling fraction of component  $i$  in cavity type  $k$ :

$$x_i^H = \frac{\theta_{large,i}v_{large} + \theta_{small,i}v_{small}}{1 + \theta_{large,i}v_{large} + \theta_{small,i}v_{small}} \quad (6)$$

where  $v$  is the fraction of cavity per water for the actual cavity type as indicated by subscripts. Corresponding mole-fraction water is then given by:

$$x_{H_2O}^H = 1 - \sum_i x_i^H \quad (7)$$

and the associated hydrate free energy is then:

$$G^{(H)} = x_{H_2O}^H \mu_{H_2O}^H + \sum_i x_i^H \mu_i^H \quad (8)$$

in which  $\mu$  denote chemical potential. Subscripts  $H_2O$  and  $i$  denote water and hydrate formers respectively. Superscripts  $H$ , water and gas denote hydrate, liquid water and gas phases respectively.  $x$  is mole-fraction in liquid or hydrate (superscript  $H$ ) and  $y$  is mole-fraction in hydrate former phase.  $T$  and  $P$  are temperature and pressure respectively and  $G$  is free energy. The  $\Delta$  symbol the change in free energy and superscript  $H_1$  indicate this hydrate formation route.

The chemical potential for guest molecule  $j$  (in the case of this work either CO<sub>2</sub> or CH<sub>4</sub>) which enters Equations (4) and (8) at equilibrium is, according to residual thermodynamics:

$$\mu_i(T, P, \vec{y}) = \mu_i^{pure,ideal\ gas}(T, P, \vec{y}) + RT \ln [y_i \phi_i(T, P, \vec{y})] \quad (9)$$

where  $y_i$  is mole-fraction of component  $i$  in the gas mixture.  $\phi_i$  is the fugacity coefficient for  $i$ . Ideal gas chemical potential for pure  $i$  can be trivially calculated for any model molecule via statistical mechanics from mass and intramolecular structure (bond lengths and bond angles). For rigid model molecules this is particularly simple and analytic though molecular weight, centre of mass and the moments of inertia. Together with density and temperature the ideal gas chemical potential is available from the momentum space canonical partition function. We have utilized the SRK [22] equation of state for calculating the fugacity coefficient, and also the density needed for the ideal gas chemical potential calculations.

The enthalpy change is trivially related to the corresponding free energy change by the thermodynamic relationship:

$$\frac{\partial \left[ \frac{\Delta G^{Total}}{RT} \right]_{P,\vec{N}}}{\partial T} = - \left[ \frac{\Delta H^{Total}}{RT^2} \right] \quad (10)$$

The superscript “Total” is introduced to also include the penalty of pushing aside the old phases. Practically the total free energy change will be the extensive version of Equation (1) plus the work needed to push away old phases in order to give space for the new hydrate phase. This penalty during the nucleation process of hydrate is interface free energy times contact area between water and hydrate forming phase. See Kvamme et al. [11] for more details. Since critical nuclei sizes are small [23–25] the whole particle can be considered as covered with water due to capillary forces. As such it is expected that interface free energy between hydrate and liquid water can be used with confidence. Above critical core size the penalty diminishes rapidly relative to the free energy change benefits as given by Equation (1).

$$\frac{\partial \left[ \frac{\mu_{H_2O}^H}{RT} \right]_{P,\vec{N}}}{\partial T} = \frac{\partial \left[ \frac{\mu_{H_2O}^{0,H}}{RT} \right]_{P,\vec{N}}}{\partial T} - \left[ \frac{\partial}{\partial T} \right]_{P,\vec{N}} \left[ \sum_{k=1,2} v_k \ln \left( 1 + \sum_i h_{ki} \right) \right] \quad (11)$$

For the liquid water phase in (1), as well as for the empty hydrate chemical potential on right hand side of (3) results are trivially obtained from Kvamme and Tanaka [16]. The second term on right hand side is reorganized as:

$$\left[ \frac{\partial}{\partial T} \right]_{P,\vec{N}} \left[ \sum_{k=1,2} v_k \ln \left( 1 + \sum_i h_{ki} \right) \right] = \left[ \sum_{k=1,2} v_k \frac{\sum_i \left[ \frac{\partial h_{ki}}{\partial T} \right]_{P,\vec{N}}}{\left( 1 + \sum_i h_{ki} \right)} \right] \quad (12)$$

and the derivatives of the cavity partition functions can be written as:

$$\left[ \frac{\partial h_{ki}}{\partial T} \right]_{P,\vec{N}} = h_{ki} \left[ -\frac{1}{RT^2} (\mu_{ki} - \Delta g_{ki}) + \frac{1}{RT} \left( \frac{\partial \mu_{ki}}{\partial T} - \frac{\partial \Delta g_{ki}}{\partial T} \right) \right] \quad (13)$$

The partial derivatives in the last term on right hand side is numerically differentiated from the polynomial fits of Kvamme and Tanaka [16]:

$$\frac{\partial \left[ \frac{\mu_{H_2O}^H}{RT} \right]_{P,\vec{N}}}{\partial T} = \frac{\partial \left[ \frac{\mu_{H_2O}^{0,H}}{RT} \right]_{P,\vec{N}}}{\partial T} + \left[ \sum_{k=1,2} v_k \frac{\sum_i h_{ki} \left[ \frac{1}{RT^2} (\mu_{ki} - \Delta g_{ki}) - \frac{1}{RT} \left( \frac{\partial \mu_{ki}}{\partial T} - \frac{\partial \Delta g_{ki}}{\partial T} \right) \right]}{\left( 1 + \sum_i h_{ki} \right)} \right] \quad (14)$$

$$H_{H_2O}^H = -RT^2 \frac{\partial \left[ \frac{\mu_{H_2O}^{0,H}}{RT} \right]_{P,\vec{N}}}{\partial T} + \left[ \sum_{k=1,2} v_k \frac{\sum_i h_{ki} \left[ (\mu_{ki} - \Delta g_{ki}) - T \left( \frac{\partial \mu_{ki}}{\partial T} - \frac{\partial \Delta g_{ki}}{\partial T} \right) \right]}{\left( 1 + \sum_i h_{ki} \right)} \right] \quad (15)$$

For liquid water the enthalpy is even more trivially obtained by numerical differentiation of the polynomial fit of chemical potential as function of T given by Kvamme and Tanaka [16].

In an equilibrium situation the chemical potential of same guest in the two cavity types must be the same and these have to be equal to the chemical potential of the same molecule in the phase that it came from. For the heterogeneous case this means chemical potential of the molecule in gas (or liquid) hydrate former phase, but outside of equilibrium the gradients in chemical potentials as function of T, P and mole-fractions have to reflect how the molecule behaves in the cavity.

Enthalpies for various guest molecules in the two types of cavities can be evaluated by Monte Carlo simulations along the lines described by Kvamme and Lund [26] and Kvamme and Førrisdahl [27] by sampling guest water interaction energies and efficient volumes from the movements of the guest molecules, i.e.,

$$H_{ki}^R = U_{ki}^R + (z_{ki} - 1)RT \quad (16)$$

where U is energy and superscript R denote residual (interaction) contribution.  $z_{ki}$  is compressibility factor for the guest molecule i in cavity k. Consistent ideal gas values for the same interaction models that were applied in calculation of the residual values is trivial:

$$z_{ki} = \frac{PV_{ki}}{k_B T} \quad (17)$$

In which  $k_B$  is Boltzmann's constant and  $V_{ki}$  is the excluded volume of a molecule of type  $i$  in cavity of type  $k$ . This latter volume is calculated from the sampled volume of center of mass movements plus the excluded volume due to water/guest occupation. Slightly more complex sampling and calculation for molecules which are not monoatomic (or approximated as monoatomic like methane) but still fairly standard [26,27] and explicit discussion on this is not needed here.

For a relevant temperature span in the order of 10 K (273 K–283 K) the differences in enthalpies as calculated from (16) using Monte Carlo sampled data does not vary substantially and can even be approximated as constant for the purpose of this work. This is as expected since the hydrate water lattice is fairly rigid and the average movements almost the same for the limited temperature range. Sampled cavity partition functions will of course vary significantly over the same temperature range due to the direct exponential (Boltzmann factor) dependency. The interaction models for CH<sub>4</sub> and CO<sub>2</sub> utilized are the same as those utilized by Kvamme and Tanaka [16]. Also note that while there is an average attraction also for CO<sub>2</sub> in small cavity, but the sampled Langmuir constant is very small and not significant. This is also confirmed by the Molecular Dynamics studies along the lines of Kvamme and Tanaka [16], for which the movements of CO<sub>2</sub> in the small cavity interferes with several water libration frequencies and the resulting free energy of inclusion is not beneficial for CO<sub>2</sub> in the small cavity. While small cavity occupation of CO<sub>2</sub> has been found at extreme conditions in the ice range of temperatures in some studies [28] it remains unclear if there would be any significant small cavity filling of CO<sub>2</sub> at all for temperatures above zero degrees Celsius. The sampled values are given in Table 1 below.

**Table 1.** Sample residual energies and cavity occupation volumes for CH<sub>4</sub> and CO<sub>2</sub>.

Property	CH <sub>4</sub>		CO <sub>2</sub>	
	Large Cavity	Small Cavity	Large Cavity	Small Cavity
$U_{ki}^R$ (kJ/mole)	−16.53	−17.73	−27.65	−10.58
$V_{ki}$ (Å <sup>3</sup> )	164.2	89.2	135.6	76.9

The energies for CO<sub>2</sub> in small cavity was sampled after a structure I containing only CO<sub>2</sub> in large cavities was stabilized. Then small cavities were gradually filled and simulations were run until the average fluctuations in sampled interaction energies were symmetrical and on average less than 0.5 per cent of the average energy for the hydrate crystal. Practically this energy value does not have any

implication on the enthalpy since the canonical partition function for CO<sub>2</sub> in small cavity is practically zero and as such also the filling fraction of CO<sub>2</sub> in small cavity is almost zero. At pressures below 95 bars along the equilibrium curve it is zero to third digit in mole-fraction while the maximum filling fraction in small cavity contributes with 0.006 to the mole-fraction at (290.00K, 403.0 bars). In contrast the calculated mole-fractions of methane in structure I varied between 0.134 at (276.16 K, 25.2 bars) along the equilibrium curve to 0.138 at (290.00 K, 164.7 bars).

The derivative of the chemical potential of a guest molecule *i* in cavity type *k* with respect to temperature as needed in Equation (26) is the negative of partial molar entropy for the same guest molecule and can be calculated according to:

$$\left[ \frac{\partial \mu_{ki}}{\partial T} \right]_{P,N} = \frac{\mu_{ki} - H_{ki}}{T} \quad (18)$$

Equation (15) can then be rearranged into:

$$H_{H_2O}^H = -RT^2 \frac{\partial \left[ \frac{\mu_{H_2O}^{0,H}}{RT} \right]_{P,N}}{\partial T} + \left[ \sum_{k=1,2} v_k \frac{\sum_i h_{ki} \left[ (H_{ki} - \Delta g_{ki} + T \frac{\partial \Delta g_{ki}}{\partial T}) \right]}{\left( 1 + \sum_i h_{ki} \right)} \right] \quad (19)$$

The sampled temperature derivatives of guest inclusion free energies for methane in small cavity exhibits a very different behaviour due to the slightly higher density (roughly 85% higher density as compared to CH<sub>4</sub> in large cavity). CO<sub>2</sub> in small cavity is not relevant since the canonical partition functions are practically zero within significance, as discussed above. The samples values for the gradient in the last term is plotted in Figure 1 below.

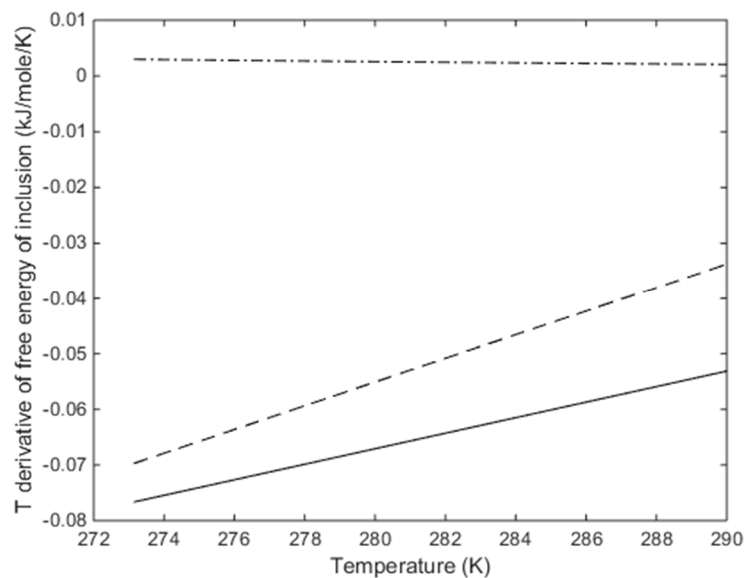


**Figure 1.** Derivatives of free energy of inclusion for CH<sub>4</sub> in large cavity of structure I (solid), CH<sub>4</sub> in small cavity of structure I (dash-dot) and CO<sub>2</sub> in large cavity of structure I (dash).

Residual enthalpies for hydrate former in a separate hydrate former phase are trivially given by:

$$H_i^R = -RT^2 \sum_i y_i \left[ \frac{\partial \ln \phi_i^{gas}}{\partial T} \right]_{P, y_j \neq i} \quad (20)$$

In which the same equation of state (SRK) is utilized as the one used for calculating fugacity coefficients for the chemical potentials. As examples we plot the calculated equilibrium curves for CH<sub>4</sub> and CO<sub>2</sub> in Figure 2a and the corresponding calculated heats of hydrate formation along the equilibrium curves in Figure 2b. The calculated results for CH<sub>4</sub> in 1a) is compared to experimental data in Kvamme et al. [11] and comparison between calculated results and experimental data for CO<sub>2</sub> equilibrium curve can be found in Kvamme [10]. What is frequently missing in reported experimental data on enthalpies of hydrate dissociation is the hydrate number. Calculated mole-fraction hydrate former along the equilibrium curves for CH<sub>4</sub> and CO<sub>2</sub> is plotted in Figure 3a and the corresponding hydrate number (mole water per mole hydrate former) is plotted in Figure 3b. As expected the trend for CH<sub>4</sub> is smooth and development as expected in terms of temperature and pressure changes along the equilibrium curve. For CO<sub>2</sub> there are distinct and expected changes after the change to high density.

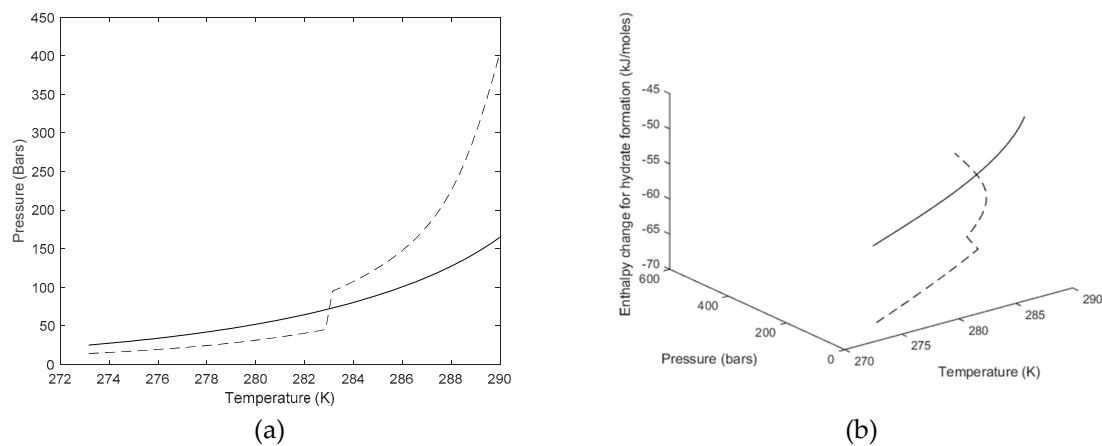


**Figure 2.** (a) Calculated equilibrium curves for CH<sub>4</sub> (solid curve) and CO<sub>2</sub> (dashed curve); (b) Calculated enthalpies of hydrate formation along the equilibrium curves for CH<sub>4</sub> (solid) and CO<sub>2</sub> (dashed).

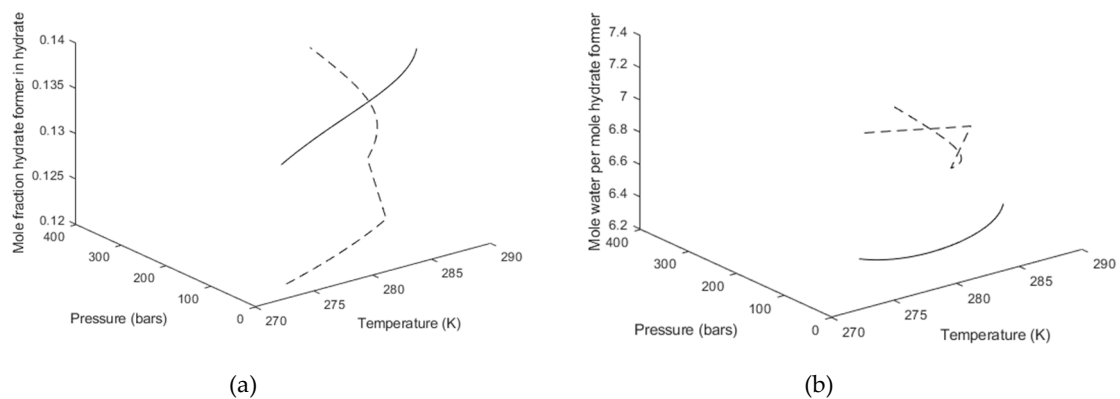


**Figure 3.** (a) Calculated mole-fraction for CH<sub>4</sub> (solid curve) and CO<sub>2</sub> (dashed curve) along the equilibrium curves. (b) Calculated hydration numbers along the equilibrium curves for CH<sub>4</sub> (solid) and CO<sub>2</sub> (dashed).

Outside of equilibrium the only phase that needs special attention is the hydrate phase since description of all fluids phase are continuous while the theory for hydrate is based on a Langmuir type of equilibrium adsorption theory:

$$G_{\text{Non-equilibrium}}^H(T, P, \vec{x}) = \left[ \begin{aligned} &G^{H,\text{Eq.}}(T^{\text{Eq.}}, P^{\text{Eq.}}, \vec{x}^{\text{Eq.}}) + \sum_r \left. \frac{\partial G^H}{\partial x_r} \right|_{P, T, x_{i \neq r}} (x_r - x_r^{\text{Eq.}}) \\ &+ \left. \frac{\partial G^H}{\partial P} \right|_{T, \vec{x}} (P - P^{\text{Eq.}}) + \left. \frac{\partial G^H}{\partial T} \right|_{P, \vec{x}} (T - T^{\text{Eq.}}) \end{aligned} \right] \quad (21)$$

in which the equilibrium properties, as reference state, is available from the calculations leading to Figure 2a. The third term on the right hand side is a trivial volume term and the final temperature term on the right hand side can be avoided by expanding in a constant temperature from the equilibrium curve. The second term involves an iteration in which a new set of filling fractions are calculated from the properties at the new pressure. the correction is very limited and no further iteration is needed. The corresponding chemical potentials needed for Equation (8) in the non-equilibrium situation is then trivially given by:

$$\mu_m^H(T, P, \vec{x}) = \left[ \frac{\partial \left( NG_{\text{Non-equilibrium}}^H(T, P, \vec{x}) \right)}{\partial N_m} \right]_{T, P, N_{k \neq m}} \quad (22)$$

which then in turn can be used for calculation of phase transition enthalpies outside of hydrate equilibrium.

## 2.2. Residual Thermodynamic Modeling of Hydrate Formation from Water and Dissolved Hydrate Former in Water

$$\Delta G^{(H_2)} = \left[ \begin{array}{l} x_{H_2O}^H \left( \mu_{H_2O}^H(T, P, \vec{x}^H) - \mu_{H_2O}^{water}(T, P, \vec{x}) \right) \\ + \sum_j x_j^H \left( \mu_j^H(T, P, \vec{x}^H) - \mu_j^{water}(T, P, \vec{x}) \right) \end{array} \right] \quad (23)$$

where the superscript  $H_2$  now refers to homogeneous hydrate formation from liquid water and dissolved hydrate former in water according to a similar notation in Kvamme et al. [11]. The chemical potential for dissolved methane in water can then [11] be formulated as:

$$\mu_{CH_4}^{water}(T, P, \vec{x}) = \mu_{CH_4}^{\infty, \text{Residual}}(T, P, \vec{x}) + \mu_{CH_4}^{\text{ideal gas}}(T, P, \vec{x}) + RT \ln \left[ x_{CH_4} \gamma_{CH_4}^{\infty}(T, P, \vec{x}) \right] \quad (24)$$

with:

$$\mu_{CH_4}^{\infty, \text{Residual}} = 3.665 + \frac{40.667}{T_R} - \frac{48.860}{T_R^2} \quad (25)$$

where  $T_R$  is temperature divided by critical temperature for methane. The maximum temperature used in the fitting is 325 K. Ideal gas as function of temperature and density is trivial to consistently calculate using the TIP4P model moments in inertia for the rotational contribution [16].

The activity coefficient for methane in water, based on the asymmetric excess convention (activity coefficient for  $CH_4$  in water unity as mole-fraction  $CH_4$  goes to zero) has been fitted to the following function:

$$\ln \gamma_{CH_4}^{\infty}(T, P, \vec{x}) = \sum_{i=1,2}^{39} \left[ a_0(i) + \frac{a_1(i+1)}{T_R} \right] (x_{CH_4})^{[0.05 + \frac{i-1}{40}]} \quad (26)$$

where  $T_R$  is reduced temperature and defined as actual  $T$  in Kelvin divided by critical temperature for methane (190.6 K). The lower summation 1,2 indicates starting from 1 and counting in steps of 2. Parameters are given by Kvamme et al. [11] (Table 3 in that paper).

For  $CO_2$  a slightly different approach is utilized. The density of  $CO_2$  as dissolved in water will correspond to the partial molar volume of  $CO_2$  at infinite dilution. The infinite dilution ideal gas chemical potential is not very sensitive to pressure so the following approximation to only temperature dependency is considered as adequate [29]:

$$\mu_{CO_2}^{\infty, \text{ideal gas}} = -130.006 + \frac{163.818}{T_{0,R}} - \frac{64.898}{T_{0,R}^2} \quad (27)$$

where  $T_{0,R}$  is 273.15 K divided by the actual temperature. Equation (11) does not apply to temperatures above 303, due to the limited range of temperatures for which infinite partial molar volumes are used, and for temperatures above 273.15 K.

The fugacity coefficient for  $\text{CO}_2$  in water is fitted to the following function:

$$\ln \phi_{\text{CO}_2}^{\text{water}}(T, P, \vec{x}) = \sum_{i=1,2}^{39} \left[ a_0(i) + \frac{a_1(i+1)}{T_R} \right] (x_{\text{CO}_2})^{[0.05 + \frac{i-1}{40}]} \quad (28)$$

where  $T_R$  is reduced temperature and defined as actual  $T$  in Kelvin divided by critical temperature for  $\text{CO}_2$  (304.35 K). The lower summation 1, 2 indicates starting from 1 and counting in steps of 2. Parameters are given in Table 2 below. The vector sign on mole-fraction  $x$  denote the vector of mole-fractions.

**Table 2.** Parameters for Equation (28).

$i$	$a_0$	$a_1$
1	-139.137483	-138.899061
3	-76.549658	-72.397006
5	-20.868725	-14.715982
7	18.030987	24.548835
9	44.210433	52.904238
11	63.353037	71.596515
13	74.713278	82.605791
15	80.411175	88.536302
17	82.710575	90.262518
19	82.017332	89.094887
21	79.373137	85.956670
23	75.429910	81.519167
25	70.680932	76.270320
27	65.490785	70.551406
29	60.126698	64.683147
31	54.782421	58.865478
33	49.592998	53.235844
35	44.500001	47.728622
37	39.869990	42.730831
39	35.597488	38.125674

The chemical potential for  $\text{CO}_2$  which applies to Equations (10) and (4) for an equilibrium case is the given by:

$$\mu_{\text{CO}_2}(T, P, \vec{y}) = \mu_{\text{CO}_2}^{\infty, \text{ideal gas}}(T, P, \vec{y}) + RT \ln \left[ x_{\text{CO}_2} \phi_{\text{CO}_2}(T, P, \vec{y}) \right] \quad (29)$$

Since the chemical potential of  $\text{CO}_2$  is not necessarily, the same for dissolved  $\text{CO}_2$  in water, and  $\text{CO}_2$  in gas (or liquid) in a non-equilibrium situation, then hydrate formed according to Equation (23) will be different from the first hydrate and accordingly denoted  $\text{H}_2$ . The composition of this hydrate will be different as seen from the corresponding compositions, which follows from Equations (4) to (8).

For homogeneous hydrate formation from liquid water and dissolved hydrate former then the number of degrees of freedom (Gibbs phase rule) is 2 and each specific set of temperature and pressure will have a maximum dissolved content of hydrate former according a Henry's law type

of calculation [11], and a minimum content of hydrate former needed to keep contacting hydrate at stability. Examples for CH<sub>4</sub> are given in Figure 4 below for CH<sub>4</sub> for a larger range of temperatures and pressures than those reported by Kvamme et al. [11] (Figure 16 in that paper). Similar results for CO<sub>2</sub> are given in Figure 5.

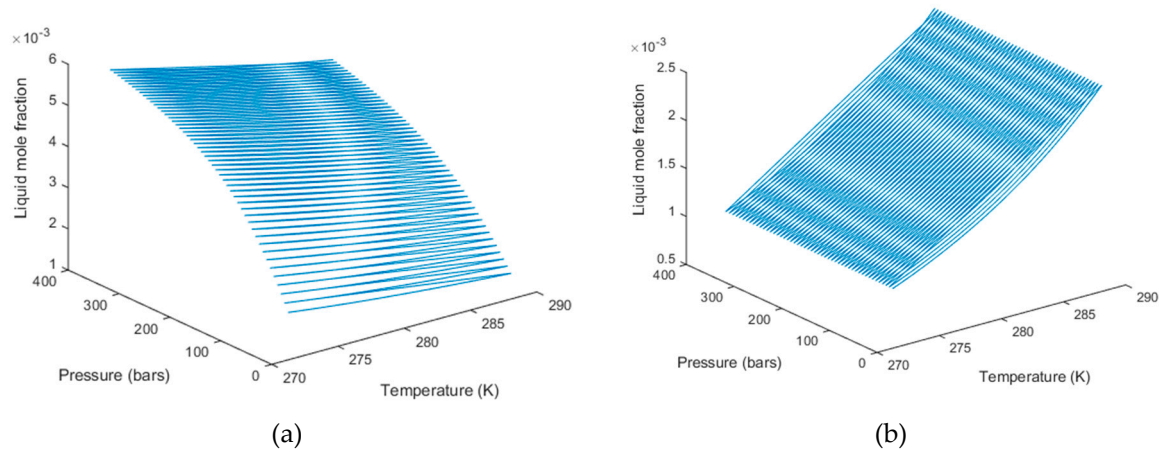


**Figure 4.** (a) Calculated solubility of CH<sub>4</sub> in water. (b) Calculated minimum limits of mole-fraction CH<sub>4</sub> in water to keep hydrate stable.

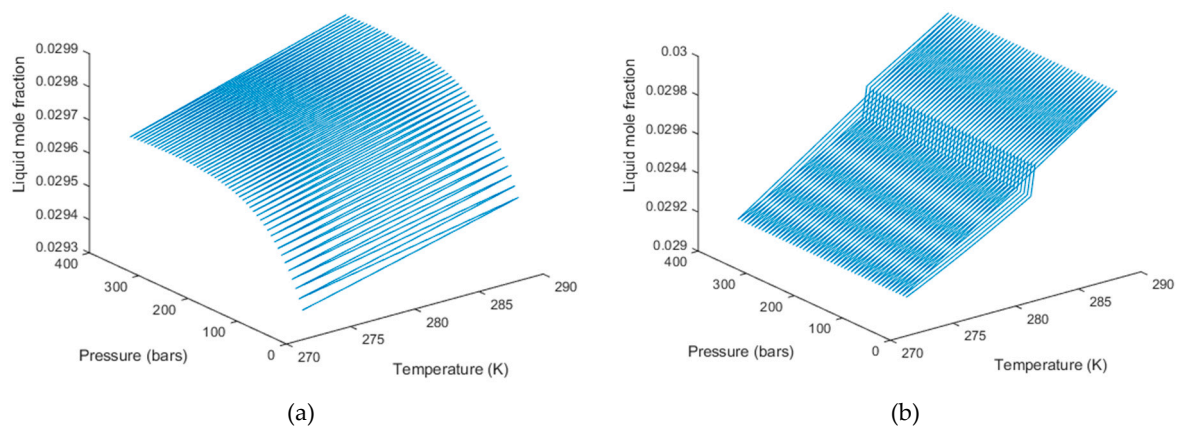


**Figure 5.** (a) Calculated solubility of CO<sub>2</sub> in water. (b) Calculated minimum limits of mole-fraction CO<sub>2</sub> in water to keep hydrate stable.

One should note the strange frames that are drawn between the corners of Figures 3b and 4b which seem to be artificial drawing in Matlab, as some straight lines drawn between the four corners in the fairly symmetric data. This might be due to the arrangement of the data from the calculations, which are in a long row of 50 temperatures for each of 50 pressures in the range from 50 to 400 bars. This is of course not a physical part of the calculated data and accordingly must be neglected in the reading of the curves.

In Figure 5b there is a fairly steep change in liquid mole-fraction for lower limit of hydrate stability, corresponding to the rapid change in density as also reflected in Figure 2a and also the rest of results illustrated in Figures 2 and 3. Methane is supercritical in these ranges of temperatures and do have any sharp density increase in the same range. The contours in Figure 4b is slightly concave, and again—the outer strange “side-walls” are not physical.

The only change in Equation (19) for this case is in the cavity partition functions so that Equation (4), now with more specific notations, can be written at equilibrium as:

$$h_{ki} = e^{\beta[\mu_{ki}^{water}(T,P,\bar{x}) - \Delta g_{ki}(T)]} \quad (30)$$

where the chemical potentials are either from Equation (24) for CH<sub>4</sub> or (29) for CO<sub>2</sub>. For the case of equilibrium it is assumed that chemical potential for the guest molecule has same chemical potential in both cavities. Outside of equilibrium then Equation (21) applies, and the Taylor expansion will also imply that the chemical potentials of guest in the two types of cavities are not necessarily the same.

A second set of changes, relative to the case of separate phases for water and hydrate former, lies in the enthalpy for the hydrate former that enters in the changes associated with the phase transition:

$$H_{CO_2}^R = -RT^2 \left[ \frac{\partial \ln \phi_{CO_2}^{water}}{\partial T} \right]_{P, y_j \neq CO_2} \quad (31)$$

and:

$$H_{CO_2}^{water} = -RT^2 \left[ \frac{\partial \left( \frac{\mu_{CO_2}^{\infty, ideal\ gas}}{RT} \right)_{P, y_j \neq CO_2}}{\partial T} + \left[ \frac{\partial \ln \phi_{CO_2}^{water}}{\partial T} \right]_{P, y_j \neq CO_2} \right] \quad (32)$$

### 3. Results

It is outside the scope of this work to provide a comprehensive review and discussion of available experimental data. That could have been natural and easy if the experimental data available were following certain standards. The problem is that all the experimental data that we have found so far in open literature is lacking some critical information and the associated error bars are uncertain. Frequent reasons for error bars are lack of information on hydrate number, no indication of pressure and lack of information on degree of super heating. For these reasons there are substantial differences in reported values for heats of dissociation between different publications. These differences are reflected in differences between reported results from various research groups even though they utilize the same experimental method. Some experimental methods are indirect in the sense that heat is not measured directly but interpreted indirectly via measurements of the pressure temperature hydrate stability limits. One example of the use of Clausius-Clapeyron is plotted in Figure 6a below. The only experimental information they utilize is the gradient of their measured equilibrium curve. Their experimental data for the pressure temperature hydrate equilibrium curve is very close to recent data, and also in accordance with Figure 2a. They utilized the calculated compressibility factor, *z*, from the SRK in the following classical version of the Clausius simplification of Clapeyron's equation:

$$\frac{\partial \ln P}{\partial \left( \frac{1}{T} \right)} = - \frac{\Delta H^{dissociation}}{zR} \quad (33)$$

Their data essentially follows a straight line as function of temperature, with the gas compressibility factor for CH<sub>4</sub> that roughly change linearly from around 0.9 at 280 K to approximately 0.85 at 282.5 K. Both end point presumably on the hydrate equilibrium pressure so that the corresponding pressures are 52 bar and 137 bars, respectively. Some other available data from open literature is plotted in as well.

Similar comparison for CO<sub>2</sub> is plotted in Figure 6b. Nasir and Lal [29] only plotted data up to 282.5 and such—the extrapolation is not fair above that temperature since they stopped before the density change for CO<sub>2</sub>. Clapeyron would not even be a fair approximation for higher temperature for several reasons; including the fact that SRK [22] is not good as calculating liquid densities (and compressibility factors) for CO<sub>2</sub>.

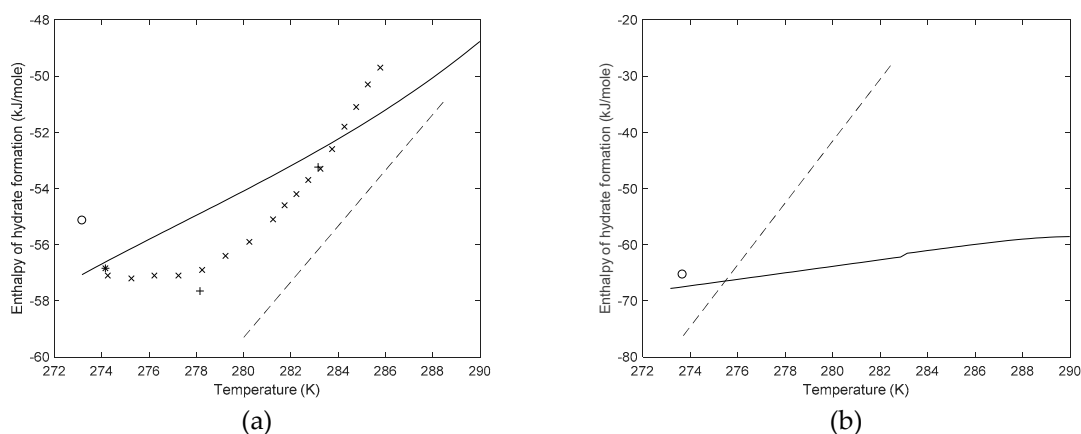


**Figure 6.** (a) Estimated heats of formation based residual thermodynamics for CH<sub>4</sub> (solid) and results from Nakamura et al. [30] (x), Deaton and Frost [31] (\*), Kang [32] (o), Lievois [33] (+) and Nasir and Lal [29] (dashed). (b) Estimated heats of formation based residual thermodynamics for CO<sub>2</sub> (solid) and results from Nasir and Lal [29] (dashed). One available value from Kang [32] is also plotted in.

#### 4. Discussion

The advantage of the proposed method for calculating enthalpies of hydrate formation is that it is totally consistent with the same residual thermodynamic models which are utilized to calculate hydrate formation equilibrium and dynamics. This includes hydrate numbers and also a route for calculating heats of formation outside of the equilibrium curve. The latter may not be as straightforward in the Clapeyron method since that method is utilizing the gradients of the P-T equilibrium curve. Reported hydrate numbers vary substantially between different reported values for heat of hydrate dissociation. Sometimes only a fixed value (independent of T and P) is used and sometimes ideal value is used. Some care have to be taken in comparing values form different group, as seen in Figure 7a,b where comparison of values per mole hydrate is in fair agreement while our values for heat of formation per mole hydrate former is lower in the case of methane hydrate. The old data from Deaton and Frost [31] is hard to evaluate in terms of accuracy based on the original source from 1946.

In general any concept based on the Clapeyron method, or the simplified Clausius-Clapeyron method, using calculated equilibrium curves, will be affected by how the pressure temperature gradient is calculated. While we use residual thermodynamics also for the empty clathrate, so as to keep these values consistent with chemical potentials for ice and liquid water, most codes today use a fitting approach in which the difference between liquid (or ice) water and empty clathrate is treated as an empirical fitting parameter. In addition to fitting parameters in the interactions between water and hydrate formers filling the cavities the fitting of chemical potential differences often goes via fitting chemical difference between water phase and empty clathrate at a reference temperature. Then a corresponding enthalpy difference is fitted in order to obtain temperature dependency for the chemical potential difference according to a relationship similar to Equation (10), which also then requires a specific heat capacity difference. And also a volume difference is needed for the pressure difference. The sum of it all results in a variety of possibilities for fitted parameters towards data experimental data. In the final end it is highly unlikely that two different codes based on this chemical potential difference route should end up with same calculations of filling fractions of various cavities in hydrates. We have no possibility to examine how large the differences will be. Experimental equilibrium curves may of course also be used, although in many cases then without any information about hydrate numbers.

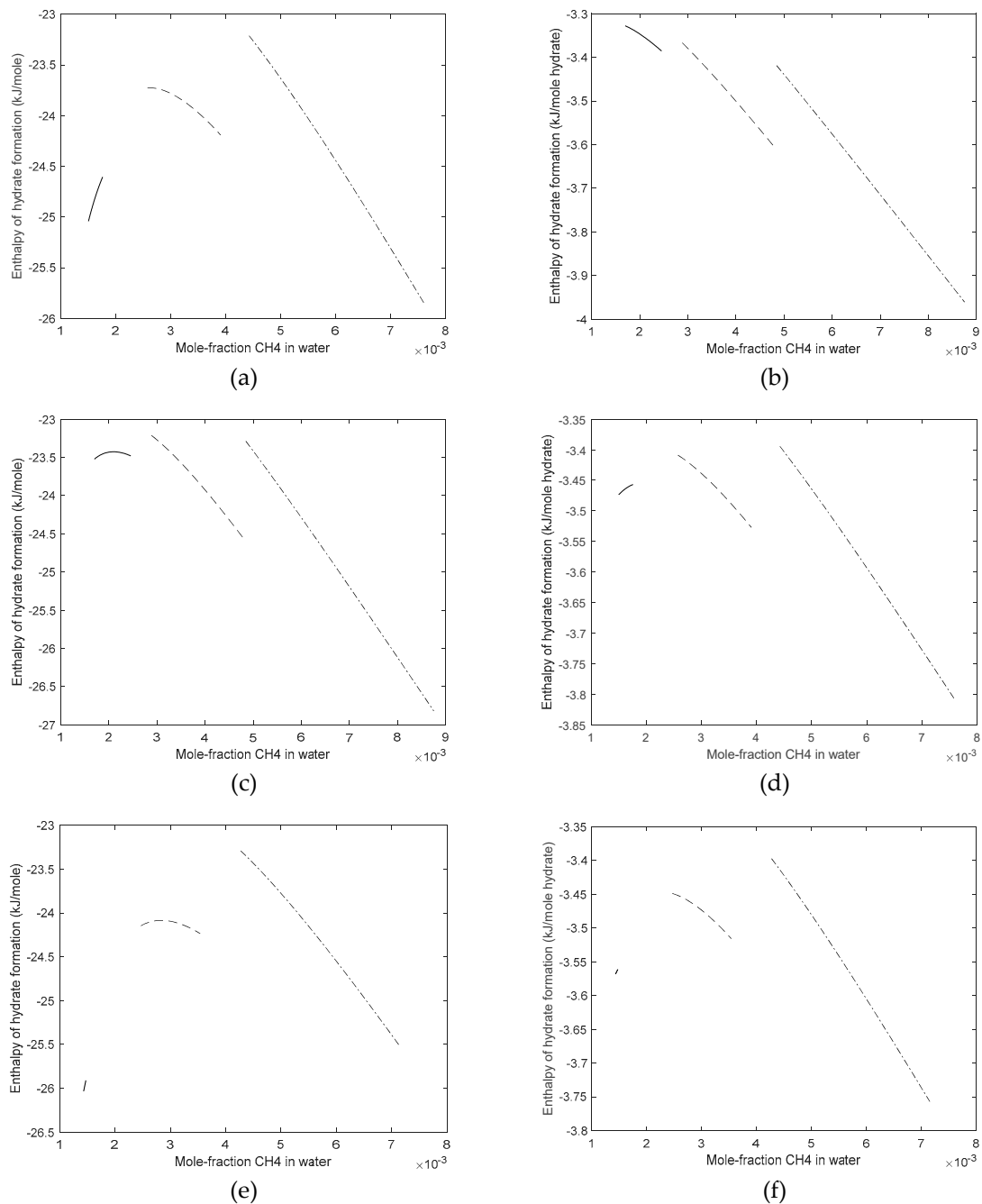


**Figure 7.** (a) Calculated enthalpies of  $\text{CH}_4$  hydrate formation at 273.16 K and three pressures. Solid curve is for 50 bars, dashed curve is for 100 bars and dash-dot is for 250 bars. (b) Same as in 8 (a) but now per mole of hydrate. (c,d) are same types of plots as (a,b) but now for 278.16 K. (e,f) are same types of plots as (a,b) but now for 280.16 K. For all the curves the mole-fraction range in each curve in each plot (each temperature and pressure) the plot ranges from maximum mole-fraction equal to solubility of  $\text{CH}_4$  in water down to minimum mole-fraction of  $\text{CH}_4$  needed to keep the hydrate stable.

What is normally not discussed much is the limited stability window of hydrate. Pressure and Temperature, like in Figure 2a is just a projection of a stability window. So even if hydrate may be inside stability range in terms of temperature and pressure it is still unstable if the outside concentration of  $\text{CH}_4$  dissolved in water is smaller than the values in Figure 4b. This can be seen clearly in Figure 7 as function of pressure. The solubility of  $\text{CH}_4$  in water at 50 bars is very low compared to the two higher pressures. The corresponding window of possible hydrate growth from solution, as given by the

distance in concentrations between 4a and 4b, narrows down when the pressures goes down to 50 bars. Similarly also the stability window for hydrate goes down with pressure. This can even be better illustrated in terms of thermodynamic driving forces (free energy change of the hydrate formation). In Figure 8 we therefore plot the values of molar (per mole hydrate) free energy changes according to Equation (23) for two temperatures and two pressures. Solubility increase with pressure and the window of hydrate formation increase from 70 bars to 200 bars for both temperatures. At 200 bars the free energy driving force at 283.16 K is roughly half that of 200 bars and 273.16 K. For 70 bars and 283.15 K the driving force is so small that it is hard to know if hydrate even can form from CH<sub>4</sub> in water solution.

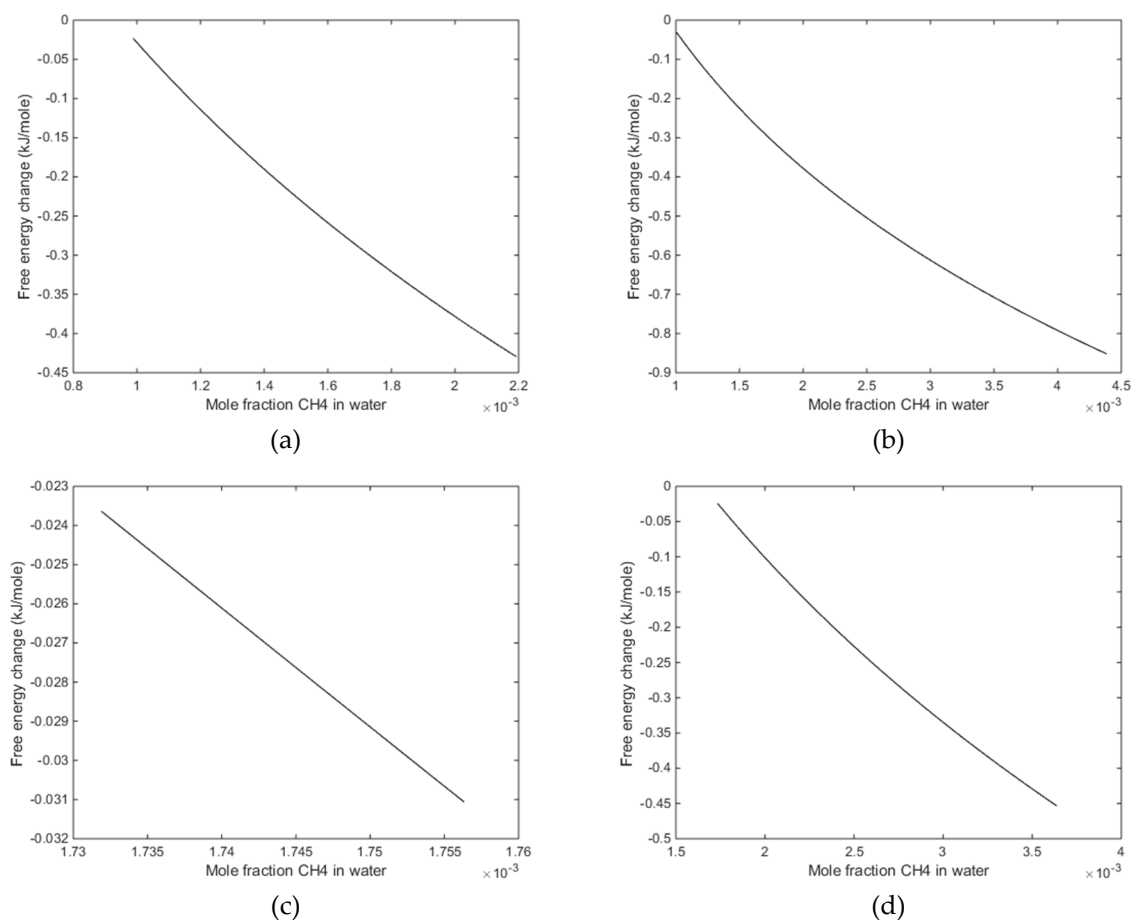


**Figure 8.** (a) Free energy change of hydrate formation in kJoule per mole hydrate formed as function of mole-fraction CH<sub>4</sub> in water at 70 bars pressure. Minimum mole-fraction CH<sub>4</sub> in surrounding water for hydrate stability is  $0.94 \cdot 10^{-3}$  and critical radius is 1.36 nm (b) same as (a) but now for 200 bars pressure. Minimum mole-fraction CH<sub>4</sub> in surrounding water for hydrate stability is  $0.94 \cdot 10^{-3}$  and critical radius is 2.69 nm (c) same as (a) but now for 283.16 K. Minimum mole-fraction CH<sub>4</sub> in surrounding water for hydrate stability is  $1.66 \cdot 10^{-3}$  and critical radius is 37.11 nm (d) same as (b) but now for 283.16 K. Minimum mole-fraction CH<sub>4</sub> in surrounding water for hydrate stability is  $1.66 \cdot 10^{-3}$  and critical radius is 2.55 nm.

The example calculations plotted in Figure 8 illustrates the limited stability window for hydrates, which is rarely discussed in open literature, which is useful in various hydrate production schemes. But dissociation towards water which is under saturated (with reference to hydrate) will dissociate hydrate. This is the reason that new fractures through hydrate always will lead to new leakage fluxes of methane. And in geological settings formation which are in risk of developing geo mechanical

instabilities and slides this route to hydrate dissociation have to be accounted for in addition to effects of temperature changes.

Another advantage is that the proposed method is applicable for all various situations of hydrate formation as long as the chemical potentials of water and hydrate formers are available. This is illustrated in this work through calculations of enthalpies of hydrate formation from aqueous solution. To our knowledge this has never been investigated theoretically before so we were not able to find neither theoretical values nor experimental data to compare with.

There is a need for a thorough analysis of available experimental data from various methods for measuring the heats of hydrate dissociation for hydrates. Both direct and indirect methods needs to be evaluated and also subjected to a sensitivity analysis so as to evaluate the relative impact of uncertainties related to unknown parameters and/or uncertainties in various key parameters. As discussed above these include hydrate number, degrees of super heating (calorimetry) and impact of applied pressure during dissociation of the hydrate. But the list can become longer as the screening proceeds. Work is in progress and expected to be submitted soon.

Yet another advantage lies in the possibility of studying hydrate nucleation towards solid surfaces. Earlier studies of water and hydrate formers [34–38] and references in these indicate that CO<sub>2</sub> may partially adsorb directly on some mineral surfaces, in competition with water, while CH<sub>4</sub> can adsorb in water layers that are structured by the interactions with the solid surface. Work is in progress on quantification of the adsorption thermodynamics so as to be able to investigate in more detail the associated kinetics of hydrate nucleation along the lines of the simplified classical theory [11] as well as modified version of our Phase Field Theory (PFT) model [7,8,39–41]. Some examples of values for adsorption chemical potential of CO<sub>2</sub> on calcite can be found in reference [36]. But several other estimated adsorption chemical potential values are available in open literature for hydrate formers and various mineral surfaces, including data from our research group. Some precautions needs to be taken since various cuttings of model minerals will unique surfaces in terms of exposed atoms and associated atomic charges. Implementation is trivial since this chemical potential enters Equations (1) and (4). Water for hydrate formation can also come from the layers adsorbed on the mineral surface, although the two first water layers of water have too low chemical potential [35] to leave adsorption in favor of hydrate formation.

As we have discussed in earlier publications most situations of hydrates in nature and industry cannot reach thermodynamic equilibrium because there are too many active phases involved in hydrate phase transitions. Hydrate forming mixtures are not uniform in thermodynamics benefits of adsorption on liquid water. Heavier components drop out first and slightly polar components (CO<sub>2</sub>, H<sub>2</sub>S). The combined first and second laws of thermodynamics will therefore also shift mixtures over to creating several hydrates with different compositions, even for heterogeneous hydrate formation from a gas mixture and liquid water. For homogeneous hydrate formation from dissolved hydrate formers in liquid water every concentration of every dissolved hydrate former will result in a unique hydrate. The proposed method does not contain any limitations in the number of hydrate formers that can be included, although the method has been demonstrated for pure components due to available data from open literature to compare the results with.

## 5. Conclusions

Available experimental data range for hydrate dissociation range from direct measurements to indirect measurements of the equilibrium curve in pressure, temperature projection and conversion of this information over to the enthalpy change of the phase transition. Approximations and lack of detailed information on all the properties needed induces various levels of bias in the reported data for heats of dissociation. We propose an alternative method using residual thermodynamics. This method is consistent with equilibrium calculations using the same thermodynamic models. An advantage of this method is that the associated entropy changes for the phase transition are consistent with the changes in free energy and enthalpy. Yet another advantage is that the method is not limited

to a system of hydrate formation from separate phases of hydrate formers and water. As we have demonstrated it can be applied for any phase transition of hydrate formation and dissociation as long as models for chemical potentials of water and hydrate formers are available. With modern tools for molecular dynamics simulations this is feasible also for studies of hydrate nucleation towards solid surfaces and other substances which may stimulate or affect hydrate nucleation. Although we have demonstrated the method for pure components there are no limits in the numbers of hydrate formers that enters hydrate.

**Funding:** This research received no external funding.

**Conflicts of Interest:** The authors declare no conflict of interest.

## References

1. Dallimore, S.R.; Uchida, T.; Collett, T.S. (Eds.) *Scientific Results from JAPEX/JNOC/GSC Mallik 2L-38 Gas Hydrate Research Well*; Geological Survey of Canada Bulletin: Mackenzie Delta, NT, Canada, 1999; Volume 544.
2. Hancock, S.H.; Collett, T.S.; Dallimore, S.R.; Satoh, T.; Inoue, T.; Huenges, E.; Hennings, J.; Weatherill, B. *Overview of Thermal-Stimulation Production-Test Results for the JAPEX/JNOC/GSC et al. Mallik 5L38 Gas Hydrate Production Research Well*; Geological Survey of Canada: Ottawa, ON, Canada, 2005; p. 585.
3. Konno, Y.; National Institute of Advanced Industrial Science and Technology (AIST), Japan. Oral Presentation at Nanotechnology and Nano-Geoscience in Oil and Gas Industry, 4–8 March 2014. Available online: <https://connect.spe.org/events/eventdescription?CalendarEventKey=7b08d694-1554-4e55-a2ce-8f5538b723fc> (accessed on 17 March 2019).
4. Tenma, N. AIST, Tokyo, Japan, Recent Status of Methane Hydrate R&D Program in Japan. In Proceedings of the Oral presentation at 11th International Methane Hydrate Research and Development, Corpus Christie, TX, USA, 5–8 December 2017.
5. Lee, H.; Seo, Y.; Seo, Y.-T.; Moudrakovski, I.L.; Ripmeester, J.A. Recovering Methane from Solid Methane Hydrate with Carbon Dioxide. *Angew. Chem. Int. Ed.* **2003**, *115*, 5202–5205. [[CrossRef](#)]
6. Falenty, A.; Genov, G.; Hansen, T.C.; Kuhs, W.F.; Salamatin, A.N. Kinetics of CO<sub>2</sub>-Hydrate Formation from Water Frost at Low Temperatures: Experimental Results and Theoretical Model. *J. Phys. Chem. C* **2010**, *115*, 4022–4032. [[CrossRef](#)]
7. Baig, K. Nano to Micro Scale Modeling of Hydrate Phase Transition Kinetics. PhD Thesis, University of Bergen, Bergen, Norway, 2017.
8. Baig, K.; Kvamme, B.; Kuznetsova, T.; Bauman, J. The impact of water/hydrate film thickness on the kinetic rate of mixed hydrate formation during CO<sub>2</sub> injection into CH<sub>4</sub> hydrate. *AIChE J.* **2015**, *61*, 3944–3957. [[CrossRef](#)]
9. Schoderbek, D.; Farrell, H.; Hester, K.; Howard, J.; Raterman, K.; Silpngarmert, S.; Lloyd Martin, K.; Smith, B.; Klein, P. *ConocoPhillips Gas Hydrate Production Test Final Technical Report 1 October 2008–30 June 2013*; DOE Award No.: DE-NT0006553; ConocoPhillips Company for United States Department of Energy National Energy Technology Laboratory: Morgantown, WV, USA, 2013.
10. Kvamme, B. Thermodynamic limitations of the CO<sub>2</sub>/N<sub>2</sub> mixture injected into CH<sub>4</sub> hydrate in the Ignik Sikumi field trial, 2016. *J. Chem. Eng. Data* **2016**, *61*, 1280–1295. [[CrossRef](#)]
11. Kvamme, B.; Selvåg, J.; Aromada, S.A.; Saeidi, N.; Kuznetsova, T. Methanol as hydrate inhibitor and hydrate activator. *Phys. Chem. Chem. Phys.* **2018**, *20*, 21968–21987. [[CrossRef](#)] [[PubMed](#)]
12. Austvik, T.; Hustvedt, E.; Gjertsen, L.H. Formation and removal of hydrate plugs—Field trial at Tommeliten. In Proceedings of the 76 Annual Meeting of the Gas Processors Association (GPA), San Antonio, TX, USA, 10–12 March 1997.
13. Gibbs, J.W. *The Collected Works of J. Willard Gibbs, Thermodynamics*; Yale University Press: New Haven, CT, USA, 1928; Volume 1, pp. 55–353.
14. Kvamme, B.; Graue, A.; Kuznetsova, T.; Gránásky, L.; Imre Tóth, G.; Pusztai, T.; Tegzeb, G. Kinetics of solid hydrate formation by carbon dioxide: Phase field theory of hydrate nucleation and magnetic resonance imaging. *Phys. Chem. Chem. Phys.* **2004**, *6*, 2327–2334. [[CrossRef](#)]

15. Tegze, G.; Pusztai, T.; Tóth, G.; Gránásy, L.; Svandal, A.; Buanes, T.; Kuznetsova, T.; Kvamme, B. Multiscale approach to CO<sub>2</sub> hydrate formation in aqueous solution: Phase field theory and molecular dynamics. *Nucleation and growth. J. Chem. Phys.* **2006**, *124*, 234710. [[CrossRef](#)]
16. Kvamme, B.; Tanaka, H. Thermodynamic stability of hydrates for ethane, ethylene, and carbon dioxide. *J. Phys. Chem.* **1995**, *99*, 7114–7119. [[CrossRef](#)]
17. Kuznetsova, T.; Kvamme, B. Grand canonical molecular dynamics for TIP4P water systems. *Mol. Phys.* **1999**, *97*, 423–431. [[CrossRef](#)]
18. Kvamme, B. Feasibility of simultaneous CO<sub>2</sub> storage and CH<sub>4</sub> production from natural gas hydrate using mixtures of CO<sub>2</sub> and N<sub>2</sub>. *Can. J. Chem.* **2015**, *93*, 897–905. [[CrossRef](#)]
19. Kvamme, B.; Kuznetsova, T.; Sapate, A.; Qorbani, K. Thermodynamic implications of adding N<sub>2</sub> to CO<sub>2</sub> for production of CH<sub>4</sub> from hydrates. *J. Nat. Gas Sci. Eng.* **2016**, *35 Pt B*, 1594–1608. [[CrossRef](#)]
20. Kvamme, B.; Kuznetsova, T.; Bauman, J.M.; Sjöblom, S.; Kulkarni, A.A. Hydrate Formation during Transport of Natural Gas Containing Water and Impurities. *J. Chem. Eng. Data* **2016**, *61*, 936–949. [[CrossRef](#)]
21. Aromada, S.A. New Concept for Evaluating the Risk of Hydrate Formation during Processing and Transport of Hydrocarbons. Master's Thesis, The University of Bergen, Bergen, Norway, 2017.
22. Soave, G. Equilibrium constants from a modified Redlich-Kwong equation of state. *Chem. Eng. Sci.* **1972**, *27*, 1197–1203. [[CrossRef](#)]
23. Buanes, T. Mean-Field Approaches Applied to Hydrate Phase Transition. PhD Thesis, University of Bergen, Bergen, Norway, 2006.
24. Svandal, A.; Kuznetsova, T.; Kvamme, B. Thermodynamic properties and phase transitions in the H<sub>2</sub>O/CO<sub>2</sub>/CH<sub>4</sub> system. *Fluid Phase Equilib.* **2006**, *246*, 177–184. [[CrossRef](#)]
25. Svandal, A. *Modeling Hydrate Phase Transitions Using Mean-Field Approaches*; University of Bergen: Bergen, Norway, 2006.
26. Kvamme, B.; Lund, A. The influence of gas-gas interactions on the langmuir-constants for some natural gas hydrates. *Fluid Phase Equilib.* **1993**, *90*, 15–44. [[CrossRef](#)]
27. Kvamme, B.; Førreisdahl, O.K. Polar guest-molecules in natural gas hydrates. *Fluid Phase Equilib.* **1993**, *83*, 427–435. [[CrossRef](#)]
28. Kuhs, W.F.; Chazallon, B.; Klapproth, A.; Pauer, F. Filling isotherms in clathrate hydrates. *Rev. High Press. Sci. Technol.* **1998**, *7*, 1147–1149. [[CrossRef](#)]
29. Nasir, K.K.Q.; Lau, K.K.; Lal, B. World Academy of Science, Engineering and Technology. *Int. J. Chem. Mol. Eng.* **2014**, *8*, 4.
30. Nakamura, T.; Makino, T.; Sugahara, T.; Ohgaki, K. Stability boundaries of gas hydrates helped by methane—Structure-H hydrates of methylcyclohexane and cis-1,2-dimethylcyclohexane. *Chem. Eng. Sci.* **2003**, *58*, 269–273. [[CrossRef](#)]
31. Deaton, W.M.; Frost, E.M., Jr. *Clathrate Hydrates and Their Relation to the Operations of Natural Gas Pipelines*; US Bureau of Mines Monograph; American Gas Association: Washington, WA, USA, 1946; Volume 8.
32. Kang, S.-P.; Lee, H.; Ryu, B.-J. Enthalpies of dissociation of clathrate hydrates of carbon dioxide. *J. Chem. Thermodyn.* **2001**, *33*, 513–521. [[CrossRef](#)]
33. Lievois, J.S.; Perkins, R.; Martin, R.J.; Kobayashi, R. Development of An Automated, High Pressure Heat Flux Calo-rimeter and its Application to Measure the Heat of Dissociation and Hydrate Numbers of Methane Hydrate. *Fluid Phase Equilib.* **1990**, *59*, 73–79. [[CrossRef](#)]
34. Kvamme, B.; Kuznetsova, T.; Pilvi-Helina Kivelæ, P.-H. Adsorption of water and carbon dioxide on Hematite and consequences for possible hydrate formation. *Phys. Chem. Chem. Phys.* **2012**, *14*, 4410–4424. [[CrossRef](#)] [[PubMed](#)]
35. Van Cuong, P. Transport and Adsorption of CO<sub>2</sub> and H<sub>2</sub>O on Calcite and Clathrate Hydrate. PhD Thesis, University of Bergen, Bergen, Norway, 2012.
36. Austrheim, M.H. Evaluation of Methane and Water Structure at a Hematite Surface—A Hydrate Prevention Perspective. Master's Thesis, University of Bergen, Bergen, Norway, 2017.
37. Nesse Knarvik, A.B. Examination of Water and Methane Structuring at a Hematite Surface in the Presence of MEG. Master's Thesis, University of Bergen, Bergen, Norway, 2017.
38. Mohammad, N. Heterogeneous Hydrate Nucleation on Calcite [1014] and Kaolinite [001] Surfaces: A Molecular Dynamics Simulation Study. Master's Thesis, University of Bergen, Bergen, Norway, 2016.

39. Kvamme, B.; Svandal, A.; Buanes, T.; Kuznetsova, T. Phase field approaches to the kinetic modeling of hydrate phase transitions. In *Natural Gas Hydrates—Energy Resource Potential and Associated Geologic Hazards*; Collett, T., Johnson, A., Knapp, C., Boswell, R., Eds.; AAPG Memoir: Tulsa, OK, USA, 2009; Volume 89, pp. 758–769.
40. Kvamme, B.; Qasim, M.; Baig, K.; Kivelä, P.-H.; Bauman, J. Phase field theory modeling of methane fluxes from exposed natural gas hydrate reservoirs. *Int. J. Greenh. Gas Control* **2014**, *29*, 263–278. [[CrossRef](#)]
41. Qasim, M. *Microscale Modeling of Natural Gas Hydrates in Reservoirs*. Ph.D. Thesis, University of Bergen, Bergen, Norway, 2012.



© 2019 by the author. Licensee MDPI, Basel, Switzerland. This article is an open access article distributed under the terms and conditions of the Creative Commons Attribution (CC BY) license (<http://creativecommons.org/licenses/by/4.0/>).